Effect of temperature on the formation of electronic bound states in an expanded bcc hydrogenoid crystal: A restricted path-integral molecular dynamics simulation

Ki-Dong Oh and P. A. Deymier

Department of Materials Science and Engineering, The University of Arizona, Tucson, Arizona 85721, USA

We have used the restricted path-integral molecular dynamics method to study the correlated electronic structure of a half-filled expanded three-dimensional hydrogenoid body-centered cubic lattice at finite temperatures. Starting from a paramagnetic metallic state with electron gas character, we find that bound electrons form upon expansion of the lattice. The bound electrons are spatially localized with their center for the motion of gyration located on ionic positions. The region of coexistence of bound and unbound states in the temperature-density plane is reminiscent of that associated with a first-order transition. At constant temperature, the number of bound electrons increases monotonously with decreasing density. The width of the region of coexistence narrows with increasing temperature.

I. INTRODUCTION

The study of strongly correlated electrons is at the very core of condensed matter physics and materials theory. For instance, great strides have been made in the understanding of the correlated electron gas because of its importance in density functional theory.[1–8] The investigation of the behavior of correlated electrons on crystalline lattices has also received a great deal of attention for its relevance to the metal to insulator transition (MIT) in several materials such as transition metal oxides.[9,10] The correlation-induced MIT, known as Mott transition, is of fundamental importance in condensed matter theory.[11] The transition results from a competition between the electrons' potential energy that tends toward localization and kinetic energy that favors delocalization. This competition is captured in a canonical lattice model for correlated electrons, namely, the half-filled Hubbard model.[12] On a lattice, the competition between the electron kinetic energy (quantified by a band width W) and the intra-atomic energy of two electrons with antiparallel spins on a given site (interaction strength U) may open a gap in the electronic energy spectrum leading to the formation of the so-called lower and upper Hubbard bands. At low values of U/W, the Hubbard model leads to a metallic state. At high values of U/W, the stable state is insulating. In this picture magnetic interactions are not taken into account and the metallic and insulating phases are paramagnetic. Magnetic interactions may provide a driving force for moments in the insulating state to long-range order, leading to a thermodynamics transformation and an antiferromagnetic insulating state below the Néel temperature.[13] A solution to the Hubbard model across the entire range of interaction strength exists only in one dimension.[13] The Mott transition in one dimension with long-range hopping has the attributes of a continuous transition with a continuous opening of the gap up to some finite value of U.[13] The Hubbard model in infinite dimension has been studied intensively since in that limit the results of mean-field approximations become exact.[13] In spite of this, a definite scenario for the Mott transition in dimensions higher than one has not been established yet.[13–23]

Correlated electrons in three-dimensional lattices have received considerably less attention than their one-dimensional (1D) and infinite dimension counterparts. There are indications that in the presence of long-range Coulomb interactions, the zero temperature Mott transition appears to be discontinuous in two and three dimensions.[24] Recently, we demonstrated the usefulness of the restricted path-integral molecular dynamics (RPIMD) method to the study of strongly correlated electrons on lattices.[25] This recent quantum molecular dynamics method is applicable to the simulation of many-fermion systems at finite temperature and includes exchange and correlation effects.[26–28] The RPIMD uses a position representation of the electrons and provides a good description of electrons that may change from delocalized to localized states. We have reported the formation of bound electronic states in a half-filled expanded 3D hydrogenoid body-centered cubic (bcc) lattice at finite temperature.[25] Starting from a metallic state, with correlated electron plasma character, we observed that bound electrons form upon expansion of the lattice. The bound electrons are spatially localized with their center for the motion of gyration located on ionic positions. The number of bound electrons increases monotonously with decreasing density.

In this paper, we study the behavior of correlated electrons on a lattice by considering Mott's original argument based on the expansion of a hydrogenoid lattice. We investigate the correlated electronic structure of the expanded 3D hydrogenoid bcc crystal at several finite temperatures. Notably, we observe that increasing temperature at constant density diminishes the weight of the conduction electrons and favors bound states on the lattice sites.

In Sec. II, we present in some details the RPIMD method and the 3D bcc hydrogenoid lattice model. The results of isothermal dilation of the crystal at several temperatures are reported and discussed in Sec. III. The paper is concluded with a summary in Sec. IV.

II. MODEL AND METHOD

We use a recent quantum molecular dynamics method applicable to the simulation of many-fermion systems at finite

temperature including correlation effects. The RPIMD method was introduced elsewhere.[26–28] This method makes use of (a) the discretized path integral representation of quantum particles as closed necklaces of P classical particles (beads or time slices in the path representation) with quantum exchange treated through crosslinking of the necklaces,[29] (b) the nonlocality of crosslinking along the necklaces,[30] (c) the restricted path integral[31] to resolve the problem of negative weights to the partition function due to exchange of indistinguishable particles.

We consider a rigid lattice of hydrogenoid ions interacting with an assembly of unpolarized electrons. This system is modeled with the classical Hamiltonian[26,27]

$$H = \sum_{k=1}^{N_{el}} \sum_{i=1}^{P} \frac{1}{2} m^*(\dot{r}_i^{(k)})^2 + \sum_{i=1}^{P} \sum_{k>l}^{N_{el}} \sum_{l=1}^{N_{el}-1} \frac{(-e)(-e/P)}{4\pi\varepsilon_o |r_i^{(k)} - r_i^{(l)}|}$$

$$+ \sum_{i=1}^{P} \sum_{k=1}^{N_{el}} \sum_{I=1}^{N_{ion}} \frac{V_{ps}(R_I - r_i^{(k)})}{P} + \sum_{k=1}^{N_{el}} \sum_{i=1}^{P} {}^* \frac{m_e P}{2\hbar^2\beta^2}$$

$$\times (r_i^{(k)} - r_{i+1}^{(k)})^2 - \frac{1}{\beta} \sum_{s=\uparrow}^{\downarrow} \frac{\sum_{i=1}^{P} \sum_{j=1}^{P} \ln \det[E_{ij}]_s \theta_{ijs}^+}{\sum_{i=1}^{P} \sum_{j=1}^{P} \theta_{ijs}^+}. \quad (1)$$

Here m^* is an arbitrary mass ($m^* = 1$ a.u.) defining an artificial kinetic energy for the dynamics of the electron necklace beads. The positions of the beads and of the ions are indicated by r and R, respectively. The second term in Eq. (1) accounts for the electron-electron Coulomb interactions. The third term is the electron-ion potential energy. The ion-electron pseudopotential is denoted V_{ps} and we use an empty core local pseudopotential[26,27] with a core radius R_c. The fourth term is the effective harmonic potential for distinguishable quantum particles.[32] The cyclic condition on the summation over the beads is denoted by an asterisk. Finally, the fifth term is an exchange potential for electron with identical spin $s = \uparrow$ or $\downarrow$. The function θ_{ij}^+ ensures the path restriction by taking on the values 1 and 0 for paths with positive and negative $\det[E_{ij}]$. All the exchange effects are included in the matrix $[E_{ij}]$ which elements are defined as $E_{ij}^{kl} = A_{ij}^{kl}/A_{ij}^{kk}$ with $A_{ij}^{kl} = \exp[-m_e P/2\beta\hbar^2 (r_i^{(k)} - r_j^{(l)})^2]$, where k and l label the electrons. The indices i and j label beads along necklaces. m_e stands for the electron mass and $\beta = 1/k_B T$.

The cubic simulation cell contains $N_{el} = 54$ ions arranged on a bcc lattice (27 unit cells) and 54 nonpolarized electrons ($N_{s=\uparrow} = 27$ and $N_{s=\downarrow} = 27$). Periodic boundary conditions are applied. The long-range Coulomb potentials in Eq. (1) are replaced by a shorter-range screened potential of the form $(1/r)\mathrm{erfc}(\eta r)$ where $\eta = 0.382$ Å^{-1}. "erfc" stands for the complementary error function. The choice of erfc as a screening function is inspired by the Ewald method.[33] Here we limit the calculation of the potential to the position-dependent real-space part of the Ewald sum. With the chosen value for η, the reciprocal-space part of the Ewald sum is negligible compared to the real-space parts.[34] For a fixed value of η, the point self-energy in the Ewald sum is independent of density and is not presented here. All potentials

are truncated at half the length of the edge of the simulation cell. The RPIMD is amenable to parallelization over the P beads.

We solve the equations of motion with a leap-frog scheme and an integration time step of 2.8×10^{-16} s. For the electron-ion pseudopotential, we employ a core radius $R_c = 1.5$ Å. R_c is large enough not to require higher corrections to Trotter formula for path-integral simulations.[35] As will be seen in the result section, R_c is small enough to lead to a significant electronic density inside the ionic core providing the on-site electron-electron interaction necessary to observe the formation of bound states. We use $P = 400$ beads for the electron necklaces in order to ensure convergence of the path integral at the temperatures and densities studied.[26,27] We eliminate all phonons by holding the ions at fixed positions. The temperature of the electrons is maintained at high enough values such that for the high densities paramagnetic metal state studied the electrons are in a nearly degenerate regime.[26,27] It is known that the simulation of stiff harmonic chains suffers from nonergodicity. To alleviate this problem, we thermostat the electron degrees of freedom by coupling every group of 54 beads (electrons) with identical label "i" to a Nosé-Hoover chain of thermostats.[36] The chain length is chosen to be five in order to lead to more randomness in the thermostating process. The first thermostat directly coupled to the electrons has a mass of 100 a.u. and the four other thermostats have a mass of 10.a.u. We have observed that this way of thermostating the electrons still yields nonergodic behavior for highly dilated crystals. To overcome this difficulty we have coupled each necklace to an Andersen's thermostat.[37] Andersen's thermostat assigns velocities distributed according to a Maxwell-Boltzmann distribution to a necklace selected randomly every 50 integration steps. We calculate the kinetic energy with two different estimators.[32,38]

Note that in the present model, spin flip is not allowed, i.e., the spin state is permanently attached to an electron. Frustration in magnetic ordering will arise from the small difference in the distance between first and second nearest neighbors in the bcc lattice compared to the deBroglie wavelength of electrons. Under the conditions of our simulations, a thermodynamic transition associated with magnetic ordering of the entire simulations cell is unlikely. Considering the spatial extend of bound electrons, the bcc lattice cannot accommodate a periodic antiferromagnetic structure with identical spin states on the first and second nearest neighbors of each site. However, the formation of small antiferromagnetic clusters is not precluded.

III. RESULTS AND DISCUSSION

We report simulations or series of simulations of the electronic structure of the hydrogenoid bcc lattice at several temperatures with lattice parameter ranging from 5.3 to 13.3 Å. Every simulation uses as starting configuration the final equilibrated configuration from a preceding simulation at either a lower temperature and identical density or same temperature but lower or higher density. As a measure of the electron density, we use the electron sphere radius expressed in units of the Bohr radius and defined by r_s
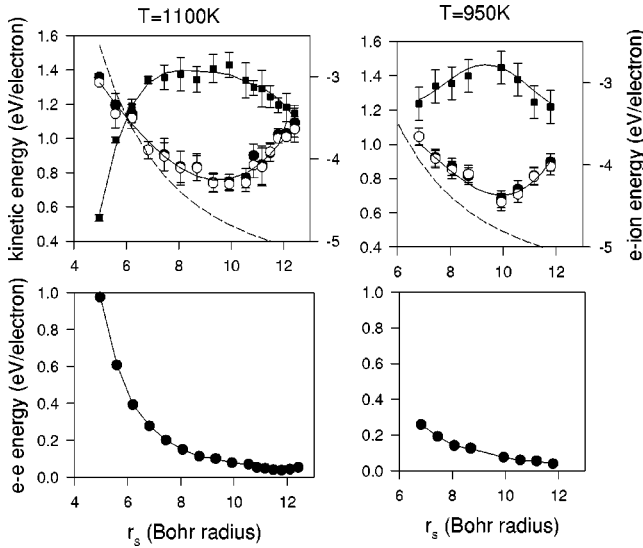
FIG. 1. (a) Average electron kinetic (circles) and electron-ion potential energy (squares) versus the electron sphere radius r_s at two temperatures. The open and closed circles are calculated with the energy estimators of Refs. 38 and 32. The solid lines are simple polynomial fits to serve as guides to the eye. The thin dashed line is the kinetic energy of the unpolarized electron plasma (Ref. 2). (b) Electron-electron (e-e) Coulomb potential energy as a function of r_s.

FIG. 2. Distributions of electron radius of gyration (see text for definition) for several densities at two temperatures.

$=[(4/3)\pi(N_{el}/V)]^{-1/3}$, where V is the volume of the simulation cell. For numerical reasons associated with arithmetic limitations on the magnitude of det[E] in Eq. (1) we could not simulate expanded systems beyond $r_s = 12.41$. The total number of MD integration time steps for the simulations ranges from 25 000 for the highest densities where equilibrium is reached fairly rapidly and up to an excess of 200 000 steps at lower density. Because of limits in computational resources, each simulation is a sequence of shorter runs of approximately 10 000 to 20 000 steps. Consequently, we estimate the standard deviation of the average energies from the set of individual average energies obtained from the short runs constituting each simulation.

To verify that our simulations had indeed reached thermodynamics equilibrium, we simulated a low-density systems, at $r_s = 11.17$, starting from a randomly generated paramagnetic insulator with only singly occupied lattice sites. The temperature was $T = 1000$ K. After the system reached equilibrium, structural and thermodynamics properties approached those of the expanded systems at the same density providing evidence that the simulations reported in this paper correspond to stable thermodynamic equilibrium.

The electron kinetic energies, electron-ion potential energy [third term in Eq. (1)] and electron-electron coulomb energy [second term in Eq. (1)] for two temperatures, $T = 950$ and 1100 K, are presented as functions of the electron sphere radius r_s in Fig. 1. The kinetic energies calculated with the two estimators agree well with each other indicating that ergodicity is satisfied. The kinetic energy is U shaped. At high density, the calculated kinetic energy follows the trend of the unpolarized uniform electron gas.[2] As density decreases, i.e., r_s increases, the electrons in the hydrogenoid
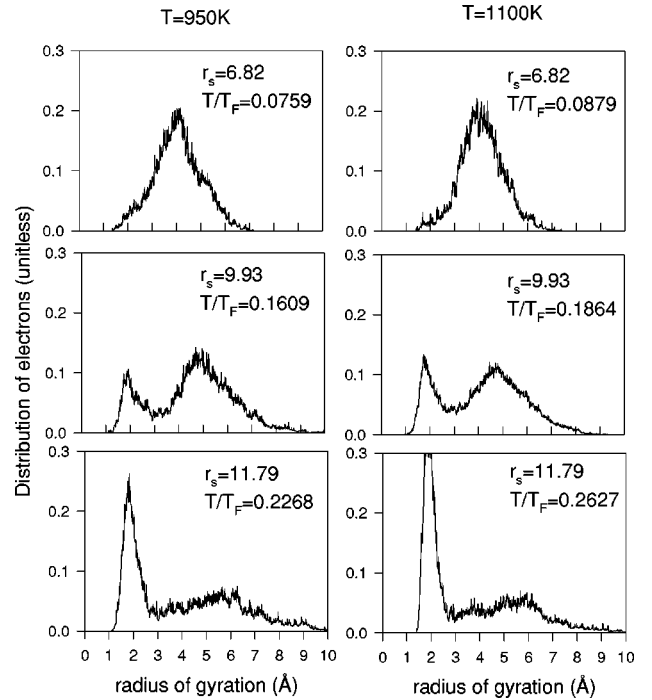
lattice deviate from the electron gas behavior. The rise in kinetic energy at low density is associated with the formation of compact electrons, i.e., highly localized electron necklaces. Figure 1(a) clearly shows that beyond $r_s = 10$, electron localization results from a competition between the rising kinetic energy and the decreasing electron-ion potential energy. The compact electrons with high kinetic energy are localizing inside the core of the ions to minimize their potential energy. The electron-electron Coulomb energy [Fig. 1(b)] decays monotonously over the range of densities studied. Beyond $r_s = 10$, the electron-electron potential energy decreases only slightly (or even appears to have reached a minimum for $T = 1100$ K) indicating that the localized electrons have effectively excluded other electrons from the ion cores.

The formation of compact electronic states is also clearly seen in Fig. 2, where we report the distribution of electrons' radius of gyration (RG) at several densities and two temperatures. The radius of gyration of an electron (k) is calculated with the following expression:

$$RG^{(k)} = \frac{1}{P}\sqrt{\sum_{i=1}^{P}(r_i^{(k)} - \bar{r}^{(k)})^2}, \qquad (2)$$

where $\bar{r}^{(k)}$ is the position of the center of mass of the electron. Parrinello and Rahman.[32] have shown that $\langle RG^2 \rangle = \hbar^2/2m_e/k_B T\, C$. For a free particle, C is equal to 1 and $\langle RG^2 \rangle$ is interpreted as the square of the average de Broglie wavelength for electrons with average momentum square $m_e k_B T$. At high density, the RG distribution takes a nearly Gaussian form with a mean RG$\sim$4 Å. For $T = 1100$ K and $r_s = 6.82$, the value of C is estimated to be $\sim$0.45 which is

nearly half that of a free particle. The electrons have some free particle character but this value for C reflects some compactness due to electron correlation as well as the interaction with the lattice. Upon a decrease in density, compact electrons form a shoulder in the RG distribution transforming into a narrow peak centered around RG$\sim$2 Å. At fixed density, the weight of bound states increases as temperature rises from 950 to 1100 K. At $T=1100$ K, the value of C for the bound electrons is now one order of magnitude less than the free electron value. This value is comparable to that of a single F center studied by Parrinello and Rahman with PIMD.[32] The compact electrons are representative of bound states since their center for the motion of gyration is located on ionic positions as illustrated by the electron-ion radial distribution functions (RDF) of Fig. 3.

In Fig. 3(a) we show that at the highest density studied $r_s\sim4.96$ decreasing the pseudopotential core radius from $R_c=2.2$ to 1.5 Å converts our system from a simple metal to an atomic lattice with overlapping atomic wave functions. In a simple metal such as potassium the e-ion RDF exhibits oscillations that have an inverse phase to the ion-ion RDF.[39] Note that the smaller amplitude of our e-ion RDF is probably due to the erfc screening of the Coulomb interactions. At $R_c=2.2$ Å, the e-ion RDF shows a minimum at $r/r_s\sim1.9$ corresponding to the closely related first- and second-nearest-neighbor distances of the bcc lattice, $r/r_s=1.76$ and 2.03, respectively. For $R_c=1.5$ Å, the e-ion RDF fills the ion core and shows a maximum in phase with the ion-ion distances. The minimum near $r/r_s=1$, indicates that the electrons occupying atomic sites start to exclude other electrons. We have also included in Fig. 3(a) the electron-proton RDF for a hot dense partially ionized atomic hydrogen fluid that also shows exclusion outside the atomic radius.[40,41] Figure 3(b) demonstrates strong electron localization within the ion cores as density decreases. The growing depression at a radius of 1 is evidence for a reduction in the number of itinerant electrons. A pictorial representation of the spatial arrangement of the localized electrons and of the free carriers within the bcc lattice is given in Fig. 4. This figure provides information somewhat similar to that of Fig. 3 but supplements it by showing that at low density, the lattice is composed of separate regions rich in bound electrons and regions rich in free carriers.

The evolution of the electronic structure of the expanded system at fixed temperature is also clearly seen in the heterospin $g_{\uparrow\downarrow}$ and homospin $g_{\uparrow\uparrow \text{ and } \downarrow\downarrow}$ electron-electron RDF reported in Fig. 5. The pair correlations are between beads of necklaces with the same label, that is, the same time slices along the discretized path representation. At high density, the electron-electron RDF calculated with the RPIMD method are characteristic of the uniform electron gas[6,26,27] with a correlation hole in the heterospin RDF and a wider exchange-correlation hole in the homospin RDF. The inset of Fig. 5, compares our results at $r_s=4.96$ with the RDF of the unpolarized uniform electron gas of Ref. 6 at a similar density calculated with variational Monte Carlo (VMC) and diffusion Monte Carlo (DMC) methods. The agreement is quite good except near the origin. The RPIMD heterospin RDF falls essentially between the VMC and DMC curves for most
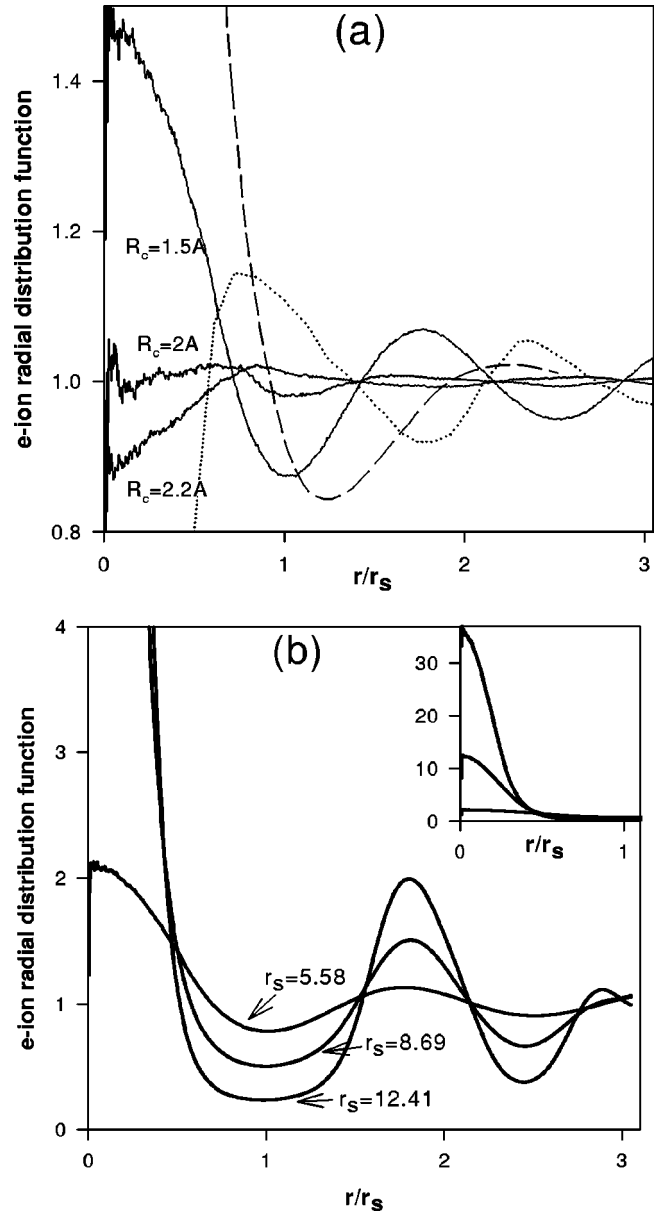

FIG. 3. (a) Electron-ion RDF at $r_s=4.96$ for several values of the pseudopotential core radii at $T=1100$ K. The dotted line is the RDF for potassium ($r_s=5.024$) extracted from Ref. 39 (inner-core structure is omitted). The dashed line is a proton-electron RDF for the partially ionized hydrogen atomic fluid of Ref. 40 ($r_s=2$). (b) Electron-ion RDF at $T=1100$ K for several electron densities. A sharpening of the peaks and growing depressions at $r/r_s\sim1$ and 2.5 indicates electron localization on the ion sites with decreasing density. The inset shows the complete distributions for radii less than the electron sphere radius.

radial distances. At very short distance, the RPIMD heterospin RDF does not take on the expected nonzero value at the origin but rapidly changes slope and dives toward 0. The discretized path integral representation of a quantum particle becomes exact as $P\rightarrow\infty$. In that limit the electron-electron Coulomb interaction term in Eq. (1), allows heterospin electrons to overlap to some extent. At finite P, this quantum effect is lost and the RPIMD method overestimates the Cou-
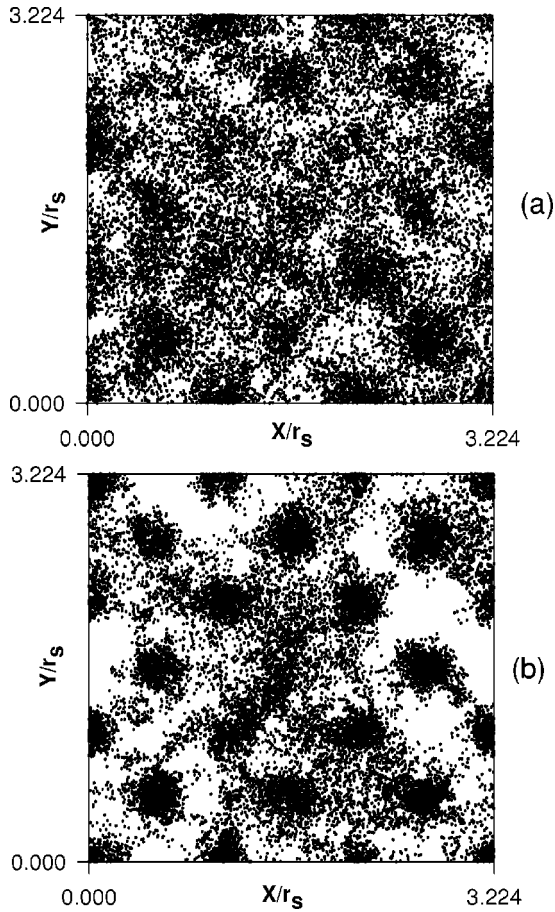
FIG. 4. Snapshot projections of the position of the nodes of all the electron necklaces on the (100) plane of the bcc lattice for two densities. The temperature is $T = 1100$ K. The electron sphere radius is (a) $r_s = 7.44$ and (b) $r_s = 11.17$.

FIG. 5. Heterospin (solid line) and homospin (dotted line) electron-electron RDF for several densities. The temperature is $T = 1100$ K. The inset compares the RPIMD RDF for the hydrogenoid lattice at $r_s = 4.96$ (solid line) with the variational (dotted line) and diffusion Monte Carlo (dashed line) results of Ref. 6 for an unpolarized uniform electron gas at $r_s = 5$. The inset shows that quantum effects are overlooked by the discrete path integral approximation ($P = 400$) only at very short radii. Because of the finite P, the heterospin RDF changes slope below approximately $r/r_s \sim 0.1$ and decreases to zero in contrast to the expected nonzero value at the origin.

lomb force between electrons at very short distance. For $P = 400$ and $r_s \sim 5$, the RPIMD method does not represent the electron-electron RDF properly for radial distances shorter than ~ 0.1 Å. This problem will not affect significantly the results presented in this paper since most of the simulations reported here are at low density for which $g_{\uparrow\downarrow}$ is very small at the origin.

As density decreases to $r_s = 8.69$, the heterospin RDF exhibits a shoulder at radial distances $r/r_s \sim 0.4$. This shoulder corresponds to doubly occupied lattice sites (i.e., singlet). This shoulder converts into a peak for lower densities indicating further spatial localization of the electrons participating in doubly occupied sites. It is worthy noting that the number of electrons in double occupancy calculated by integrating $g_{\uparrow\downarrow}(r)$ over the interval $0 < r/r_s < 1$ does not amount to more than a fraction of an electron. The homospin RDF shows also a shoulder at $r/r_s \sim 0.7$ that results from a nonzero but very small number of doubly occupied triplet sites. Upon dilation of the lattice the increasing number of singly occupied lattice sites yields a sharper peaks in the RDF encompassing both the nearest-neighbor distance of the bcc lattice and the second-nearest-neighbor distance.

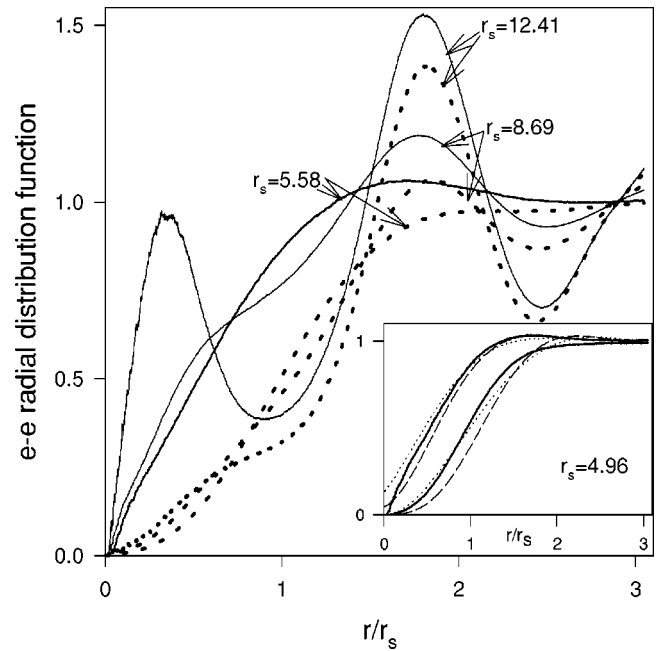The transfer of spectral weight from the free carrier states to the bound electron states as temperature is increased at fixed density ($r_s = 8.69$) is unambiguously confirmed in Fig. 6. It is worthy noting that there exists a similarity between the distribution at $T = 1300$ K, $r_s = 8.69$ and the distribution of Fig. 2 at $T = 950$ K and $r_s = 9.93$. This similarity shows that the relevant energy scale for the formation of bound states upon expansion is the Fermi temperature T_F. Indeed, despite their different temperatures and densities, these two systems have very similar values of T/T_F. The inset of Fig. 6 summarizes the spectral reweighing between unbound and bound states. We calculated the number of bound electrons by integrating a Gaussian fit to the first peak in the distribution of RG. The number of free carriers is the difference between the total number of electrons (i.e., 54) and the number of bound electrons. At a constant density, the % of unbound electron decreases as T increases. This implies that for $r_s = 8.69$, the single particle density of state at the Fermi energy is nonzero and that it decreases as temperature increases.

Our observations are compatible with the predictions of the Hubbard model concerning the single particle excitation spectrum (SPES).[22,42] Upon increase of U/W (our simulations correspond to a fixed U and a W decreasing with increasing r_s) from the paramagnetic metal, the SPES develops a central peak flanked by Mott's sidebands. The central peak is located at the Fermi liquid value. At equilibrium, electrons occupying the central peak are free carriers, while electrons occupying states in the lower sideband exhibit
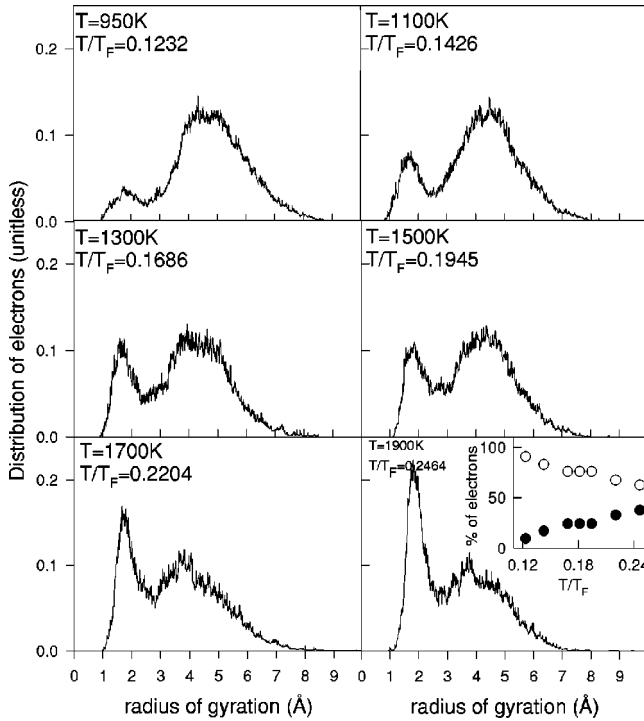
FIG. 6. Distributions of electron radius of gyration for a crystal with $r_s = 8.69$ at several temperatures. The inset reports the % of electrons in bound states (closed circle) and of free carriers (open circle) as a function of temperature.
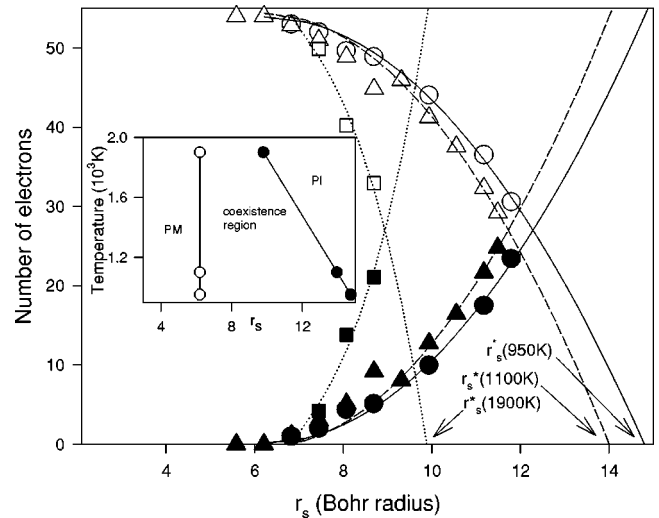

FIG. 7. Number of bound electrons (filled symbols) and unbound electrons (open symbols) at three temperatures ($T = 950$ K, circles; $T = 1100$ K, triangles; and $T = 1900$ K, squares). r_s^* corresponds to the density at which all the electrons ought to have transformed to bound states and is used to construct the temperature-density phase diagram in the inset. PM and PI stand for paramagnetic metal and paramagnetic insulator, respectively.

more boundlike behavior. Rare doubly occupied sites correspond to the electrons in the upper sideband. As temperature increases the spectral weight of the free-carrier central peak diminishes rapidly.[15,22,42] This results in a transfer of spectral weight to the side bands.

Finally, we report in Fig. 7 the calculated number of bound and unbound electrons at the three temperatures (950, 1100, and 1900 K) at which density was varied systematically over a wide range of values. The number of bound electrons is estimated from the first peak in the distributions of RG as mentioned before. At all three temperatures, the number of bound electrons increases with decreasing density, i.e., increasing r_s. Independently of temperature, at least to the level of resolution of our calculations, bound electronic states appear at $r_s \sim 6$ corresponding to an electron density $n = 6.75 \times 10^{-3}$ Å^{-3}. This density is in good agreement with Mott's criterion for the formation of bound states[43] $n^{1/3} r_H > 0.4$.

The RPIMD method did not allow us to expand the bcc lattice beyond $r_s \sim 12$. However, we can estimate the density at which all the electrons ought to be localized on ionic sites, that is, the density for completion of the transition from a paramagnetic metal to a paramagnetic insulator. For this, we fit the calculated number of bound electrons at the three temperatures to monotonously increasing functions that reach the value 0 at $r_s = 6.2$. The choice of a continuous function for this fit is motivated by the observation of Kohn and Majumdar that the transition from unbound to bound states in a noninteracting Fermi gas occurs with continuous change of the properties.[44] These authors conclude, however, that the

properties may not vary continuously if one has strong interaction between the electrons as is the case here. The inset of Fig. 7 summarizes our findings in the form of a temperature-density phase diagram. This diagram shows two phase boundaries. A boundary, nearly independent of temperature, separates the paramagnetic metallic (PM) state from the region where bound and free carriers coexist. The second boundary separates the coexistence region and the paramagnetic insulting (PI) state. The width of the coexistence region narrows as temperature increases suggesting that the transition may be of first order[45] in accord with several studies of the Hubbard model.[17–22] Indeed, a cross over transition would imply that the width of the coexistence region increases with temperature.[13] The temperature dependence of the phase boundaries in our T versus r_s phase diagram shows similar trends observed in T versus U/W phase diagrams for the Hubbard model in infinite dimensions;[20,21] namely, a significantly weaker temperature dependence of the PM-coexistence region boundary compared to the boundary between the PI and the coexistence regions.

IV. CONCLUSIONS

We have reported a study of the correlated electronic structure of an expanded 3D hydrogenoid bcc lattice. The electronic structure is modeled within the frame of the RPIMD method that enables the simulation of quantum particles with exchange and correlation effects at finite temperature. The electronic structure of the bcc lattice is characterized via electron-ion, electron-electron RDF, as well as distributions of the electron's radius of gyration. The results presented in this paper suggest that the transition from a paramagnetic metal, with no bound states, to a paramagnetic

insulator, with no free carriers, may possess a first-order character. In qualitative accord with density-functional calculations of hydrogen plasma,[46] path-integral Monte Carlo simulations,[47] and variational density matrix method[47] for hot, dense hydrogen, we find that bound electronic states begin to appear as the density of the hydrogenoid lattice is

lowered and temperature is raised. This observation is an encouraging success for the RPIMD simulation of strongly correlated electron systems. We anticipate that improvements in the method and its extension to include for instance phonons will provide a tool for shedding new light on systems with many interacting electrons.

[1] M. Gell-Mann and K. Bruekner, Phys. Rev. **106**, 364 (1957).

[2] D.M. Ceperley, Phys. Rev. B **18**, 3126 (1978).

[3] D.M. Ceperley and B.J. Alder, Phys. Rev. Lett. **45**, 566 (1980).

[4] F. Perrot and M.W.C. Dharma-wardana, Phys. Rev. A **30**, 2619 (1984).

[5] R.G. Dandrea, N.W. Ashcroft, and A.E. Carlsson, Phys. Rev. B **34**, 2097 (1986).

[6] G. Ortiz and P. Ballone, Phys. Rev. B **50**, 1391 (1994).

[7] F. Perrot and M.W.C. Dharma-wardana, Phys. Rev. B **62**, 16536 (2000).

[8] F. Perrot and M.W.C. Dharma-wardana, Phys. Rev. Lett. **87**, 206404 (2001).

[9] T. Arima, Y. Tokura, and J.B. Torrance, Phys. Rev. B **48**, 17 006 (1993).

[10] J.S. Ahn, J. Bak, H.S. Choi, T.W. Noh, J.E. Han, Y. Bang, J.H. Cho, and Q.X. Jia, Phys. Rev. Lett. **82**, 5321 (1999).

[11] N.F. Mott, *Metal-Insulator Transitions*, 2nd ed. (Taylor and Francis, London, 1990).

[12] J. Hubbard, Proc. R. Soc. London, Ser. A **276**, 238 (1963).

[13] F. Gebhard, *The Mott Metal-Insulator Transition: Models and Methods* (Springer, Berlin, 1997).

[14] E. Kalinowski and F. Gebhard, J. Low Temp. Phys. **126**, 979 (2002).

[15] Ph. Nozière, Eur. Phys. J. B **6**, 447 (1998).

[16] D.E. Logan and P. Noziéres, Philos. Trans. R. Soc. London, Ser. A **356**, 249 (1998).

[17] M. Rozenberg, G. Kotliar, and X.Y. Zhang, Phys. Rev. B **49**, 10 181 (1994).

[18] A. Georges, G. Kotliar, W. Krauth, and M.J. Rozenberg, Rev. Mod. Phys. **68**, 13 (1996).

[19] G. Kotliar, J. Low Temp. Phys. **126**, 1009 (2002).

[20] Ning-Hua Tong, Shun-Qing Shen, and Fu-Cho Pu, Phys. Rev. B **64**, 235109 (2001).

[21] R. Bulla, T.A. Costi, and D. Vollhardt, Phys. Rev. B **64**, 045103 (2001).

[22] J. Schlipf, M. Jarrell, P.G.J. van Dongen, N. Blumer, S. Kehrein, Th. Pruschke, and D. Vollhardt, Phys. Rev. Lett. **82**, 4890 (1999).

[23] R. Noack and F. Gebhard, Phys. Rev. Lett. **82**, 1915 (1999).

[24] R. Chitra and G. Kotliar, Phys. Rev. Lett. **84**, 3678 (2000).

[25] P.A. Deymier and Ki-Dong Oh, Modell. Simul. Mater. Sci. Eng. **12**, 197 (2004).

[26] Ki-Dong Oh and P.A. Deymier, Phys. Rev. B **58**, 7577 (1998).

[27] Ki-Dong Oh and P.A. Deymier, Phys. Rev. Lett. **81**, 3104 (1998).

[28] Ki-Dong Oh and P.A. Deymier, Phys. Rev. B **59**, 11 276 (1999).

[29] D. Chandler and P.G. Wolynes, J. Chem. Phys. **74**, 4078 (1981).

[30] R.W. Hall, J. Chem. Phys. **89**, 4212 (1988); **93**, 5628 (1989); **91**, 1926 (1989).

[31] D.M. Ceperley, Phys. Rev. Lett. **69**, 331 (1992).

[32] M. Parrinello and A. Rahman, J. Chem. Phys. **80**, 860 (1984).

[33] C. Kittel, *Introduction to Solid State Physics*, 6th ed. (Wiley, New York, 1986).

[34] P. Linse and H.C. Andersen, J. Chem. Phys. **85**, 3027 (1986).

[35] X-P Li and J.Q. Broughton, J. Chem. Phys. **86**, 5094 (1987).

[36] G.J. Marthyna and M.L. Klein, J. Chem. Phys. **97**, 2635 (1992).

[37] H.C. Andersen, J. Chem. Phys. **72**, 2384 (1980).

[38] M.F. Herman, E.J. Bruskin, and B.J. Berne, J. Chem. Phys. **76**, 10 (1982).

[39] S. Kambayashi and J. Chihara, Phys. Rev. E **53**, 6253 (1996).

[40] W.R. Magro, B. Militzer, D.M. Ceperley, B. Bernu, and C. Pierleoni, in *Strongly Coupled Coulomb Systems*, edited by G.J. Kalman, J.M. Rommel, and K. Blagoev (Plenum Press, New York, 1998).

[41] B. Militzer and E.L. Pollock, Phys. Rev. E **61**, 3470 (2000).

[42] G. Kotliar, E. Lange, and M. Rozenber, Phys. Rev. Lett. **84**, 5180 (2000).

[43] N.F. Mott, Philos. Mag. **6**, 287 (1961).

[44] W. Kohn and C. Majumdar, Phys. Rev. **138**, A1617 (1965).

[45] H.B. Callen, *Thermodynamics and an Introduction to Thermostatistics*, 2nd ed. (Wiley, New York, 1985).

[46] M.W.C. Dharma-wardana and F. Perrot, Phys. Rev. A **26**, 2096 (1982).

[47] W.R. Magro, D.M. Ceperley, C. Pierleoni, and B. Bernu, Phys. Rev. Lett. **76**, 1240 (1996).